Photogenerated exciton-breather state in *trans*-polyacetylene

C. L. Wang and F. Martino
Department of Physics, The City College of The City University of New York, New York, New York 10031
(Received 9 April 1986)

We perform a dynamical simulation of photogenerated excitations in *trans*-polyacetylene by using the Su-Schrieffer-Heeger extended Hubbard model. We find that two possible excited states may be photogenerated depending on the energy gained by the system. If the system energy is higher than a critical value, soliton-antisoliton pairs are photogenerated and are free to separate, leaving behind a central breather mode. If the system energy is lower than the critical value, the soliton-antisoliton pairs will bind and form a different central oscillation: an exciton-breather. The critical energy is slightly above the soliton pair-creation energy. We discuss our results and compare with experiment.

INTRODUCTION

It is well known[1-4] that the Coulomb interaction plays an important role in the formation of the soliton in *trans*-polyacetylene [*trans*-$(CH)_x$]. Many authors[5-8] have discussed the static effect of electron-electron Coulomb interaction in the framework of the Su-Schrieffer-Heeger (SSH) Hamiltonian,[9] but dynamical effects have as yet not been considered. Recently, Rice and Howard[10,11] indicated through a semiphenomenological calculation that photogenerated solitons will bind and form a solitonic exciton. Grabowski, Hone and Schrieffer[8] found analytically through a first-order perturbation treatment that there exists an excitonic bound state which has lower potential energy than a well-separated soliton-antisoliton pair, and they concluded that oppositely charged soliton-antisoliton pairs do form excitonlike bound states.

Recently experimental findings[12-15] support these conclusions. The strong temperature dependence of the photoconductivity and the absorption peak observed at 1.35 eV suggest that the photoexcited electron-hole pairs decay into different excited states at different temperatures. The infrared absorption peaks at about 500 cm^{-1} in *trans*-$(CH)_x$ and at 400 cm^{-1} in *trans*-$(CD)_x$, which were assigned to the pinned translation mode of the soliton by comparison with infrared spectra of chemically doped samples, may be interpreted as vibrational modes around the excitonlike bound state.

Many numerical dynamical simulations[16-19] have been performed using the pure SSH model to explore the dynamical features of soliton formation. Perhaps the most interesting one is the work done by Bishop *et al.*[19] They found that the soliton has a maximum velocity on the order of the sound velocity, and thus the kinetic energy has an upper limit, and the excess energy of the system forms a breather, leaving behind well-separated photogenerated solitons. They claim this breather to be responsible for the 1.35 eV absorption peak. However, since there is no essential difference between photogeneration and doping in the pure SSH model calculation, and the 1.35 eV absorption peak is absent in the case of doping, it is necessary to include the effect of electron-electron interactions in order to adequately test this claim.

In this paper we present our dynamical simulation results for photogeneration in the presence of electron-electron interaction in *trans*-polyacetylene. We find that a photo-induced electron-hole pair may decay into an exciton-breather state if the system energy is less than the creation energy of a well-separated soliton pair and greater than that of the excitonic bound state. (The system energy is measured with respect to that of the perfectly dimerized ground state in this paper.) It is necessary here to draw a clear distinction between this "exciton-breather state" and the central breather found by Bishop *et al.*[19] The exciton breather is a symmetric oscillation of the bound soliton pair along the chain about the exciton center. Such a mode is also found in photoexcited states of nondegenerate linear chains.[20] If the system energy is above the soliton pair-creation energy, the soliton pairs are generated and the central breather mode of the separated soliton-antisoliton pair is created. The soliton pairs are not free to separate, however, unless the system energy is large enough. In the following sections we present the model Hamiltonian, the numerical technique, and the main results, respectively. A discussion is presented in the final section.

MODEL HAMILTONIAN

The model Hamiltonian employed for our calculation is the standard SSH Hamiltonian with added extended Hubbard terms. These include two terms, an on-site electron-electron term and a nearest-neighbor interaction term. Only the first neighbor term is considered

$$H = H_0 + H_1 , \tag{1a}$$

$$H_0 = -\sum_{n,\sigma} t_n (c^{\dagger}_{n+1,\sigma} c_{n,\sigma} + \text{H.c.}) + \tfrac{1}{2} K \sum_n (u_{n+1} - u_n)^2 + \tfrac{1}{2} M \sum_n \dot{u}_n^2 , \tag{1b}$$

$$H_1 = U \sum_n c^{\dagger}_{n\uparrow} c_{n\uparrow} c^{\dagger}_{n\downarrow} c_{n\downarrow} + V \sum_{n,\sigma,\sigma'} c^{\dagger}_{n,\sigma} c_{n\sigma} c^{\dagger}_{n+1,\sigma'} c_{n+1,\sigma} , \tag{1c}$$

with

$$t_n = t_0 + \alpha (u_n - u_{n+1}) , \tag{1d}$$

where $c^{\dagger}_{n,\sigma}$ and $c_{n,\sigma}$ are the creation and annihilation operators of electrons with spin σ on site n, respectively; t_0 is the hopping integral for the undimerized case and α is the electron-phonon coupling constant, with u_n representing the displacement from the undimerized position of the nth (CH) group; K is the lattice spring constant and M is the mass of the (CH) group. The coefficients U and V represent the strengths of the Coulomb interaction.

Dimerization owing to Peierls instability opens a gap in the π energy band structure at the Fermi surface. The number of π electrons of the system is equal to that of the sites, and all the π electrons are in the valence band below the gap in the ground state. The ground state is degenerate, and this degeneracy is not destroyed by the Coulomb interaction. Thus the condition for generation of solitons remains. After an electron-hole pair is photogenerated the single electron spectrum is changed by the lattice distortion. The system potential energy is lowered and a charged soliton-antisoliton pair is formed. The single electron-energy spectrum in the presence of soliton pairs has two localized levels located symmetrically with respect to the gap center. These two levels are shifted from the top of the valence band and the bottom of the conduction band. Each of them is singley occupied with opposite spins.

The photogeneration of neutral soliton pairs is forbidden in the direct process and is almost forbidden in the indirect process.[21–23] Oppositely charged soliton-antisoliton pairs can be generated and can be described using the following spin-singlet state,[22,8]

$$\Psi_x=(\Psi_{+-}+\Psi_{-+})/\sqrt{2}\ , \tag{2a}$$

with

$$\Psi_{\alpha\beta}=c^{\dagger}_{\alpha\uparrow}c^{\dagger}_{\beta\downarrow}\,|\,V\rangle \tag{2b}$$

and

$$|\,V\rangle=\prod_k c^{\dagger}_{k\uparrow}c^{\dagger}_{k\downarrow}\,|\,0\rangle\ , \tag{2c}$$

where $c^{\dagger}_{+\sigma}$ ($c^{\dagger}_{-\sigma}$) is the creation operator of an electron with spin σ in a bonding (antibonding) localized state with the energy lower (higher) than the gap center, and the operator $c^{\dagger}_{k\sigma}$ creates an electron with spin σ in the molecular orbital k inside the valence band, which is fully occupied by $N-2$ spin-paired electrons, where N is the number of π electrons of the system and is even.

Following Ref. 8, we first transform the site electron operators into molecular-orbital operators,

$$c_{n,\sigma}=\sum_{k'} a^{k'}_{n\sigma}c_{k'\sigma}\ . \tag{3}$$

Here the summation of k' is over the entire electron spectrum. Since the electron distributions for each spin are the same in this case, the spin degeneracy of the single electron energy is maintained. We will drop the spin subscript σ below. Then the electron part of the system energy of the excited state Ψ_x can be obtained directly,

$$E^{\rm el}=\langle\Psi_x\,|\,H^{\rm el}\,|\,\Psi_x\rangle=\varepsilon_0+\varepsilon_c\ , \tag{4a}$$

with the Hartree-Fock part,

$$\varepsilon_0=\tfrac{1}{2}(\langle\Psi_{+-}\,|\,H^{\rm el}\,|\,\Psi_{+-}\rangle+\langle\Psi_{-+}\,|\,H^{\rm el}\,|\,\Psi_{-+}\rangle)\ , \tag{4b}$$

and the correlation part

$$\varepsilon_c=\tfrac{1}{2}(\langle\Psi_{+-}\,|\,H^{\rm el}\,|\,\Psi_{-+}\rangle+\langle\Psi_{-+}\,|\,H^{\rm el}\,|\,\Psi_{+-}\rangle)\ . \tag{4c}$$

To write the explicit results in a short form, we define charge-density parameters and bond parameters at each site as

$$\begin{aligned} D^{\nu}_n&=\sum_k |\,a^k_n\,|^2\ ,\\ D^{+}_n&=D^{\nu}_n+|\,a^{+}_n\,|^2\ ,\\ D^{-}_n&=D^{\nu}_n+|\,a^{-}_n\,|^2\ , \end{aligned} \tag{5a}$$

$$\begin{aligned} P^{\nu}_n&=\sum_k (a^k_n)^*a^k_{n+1}\ ,\\ P^{+}_n&=P^{\nu}_n+(a^{+}_n)^*a^{+}_{n+1}\ ,\\ P^{-}_n&=P^{\nu}_n+(a^{-}_n)^*a^{-}_{n+1}\ , \end{aligned} \tag{5b}$$

where k is summed over the valence band. The electron energy can be expressed as,

$$\begin{aligned} \varepsilon_0=\tfrac{1}{2}\Bigg[&-\sum_n t_n[P^{+}_n+(P^{+}_n)^*]-\sum_n t_n[P^{-}_n+(P^{-}_n)^*]\Bigg]\\ &+U\sum_n D^{+}_nD^{-}_n+V\sum_n (D^{+}_nD^{-}_{n+1}+D^{-}_nD^{+}_{n+1}\\ &\qquad +D^{+}_nD^{+}_{n+1}+D^{-}_nD^{-}_{n+1}\\ &\qquad -|\,P^{+}_n\,|^2-|\,P^{-}_n\,|^2)\ , \end{aligned} \tag{6a}$$

$$\varepsilon_c=U\sum_n |\,a^{+}_n\,|^2\,|\,a^{-}_n\,|^2+2V\sum_n (a^{-}_n)^*a^{+}_n(a^{+}_{n+1})^*a^{-}_{n+1}\ . \tag{6b}$$

NUMERICAL TECHNIQUE

In order to calculate the single electron-energy spectrum, we make use of the mean-field approximation to get the effective Hamiltonian of the electrons.

$$\begin{aligned} H^{\rm el}_{\rm eff}=\sum_{n,\sigma}\Bigg[&\left(-t_n-V\frac{P^{+}_n+P^{-}_n}{2}\right)c^{\dagger}_{n+1,\sigma}c_{n,\sigma}+{\rm H.c.}\Bigg]\\ &+\sum_{n,\sigma}\Bigg[U\frac{D^{+}_nD^{-}_n}{2}+V(D^{+}_{n+1}+D^{-}_{n+1}\\ &\qquad +D^{+}_{n-1}+D^{-}_{n-1})\Bigg]c^{\dagger}_{n,\sigma}c_{n,\sigma}\ . \end{aligned} \tag{7}$$

To eliminate end effects the periodical boundary conditions are used, $D^{\pm}_{N+1}=D^{\pm}_1$, $D^{\pm}_0=D^{\pm}_N$. The matrix form

of $H_{\rm eff}^{\rm el}$ is Hermitian and tridiagonal. It can be diagonalized by a unitary matrix $\underline{A}$, whose elements a_n^k are the ones defined in Eq. (3). Since the elements of the matrix

$$h_{n',n} \equiv \langle 0 \mid c_{n'} H_{\rm eff}^{\rm el} c_n^\dagger \mid 0 \rangle$$

contain a_n^k the matrix equation can be iterated to obtain self-consistency. On practice, we find that a self-consistent result can be obtained if we assume the matrix is real and symmetric. This means $P_n^\pm$ are real and the transformation matrix $\underline{A}$ is real orthogonal, which is consistent with the original assumption. We also find that charge-conjugation symmetry is not broken in this particular case when the Coulomb terms are included. This symmetry can be seen from Eq. (7). If we assume $D_n^+ = D_n^- = \frac{1}{2}$ in the $H_{\rm eff}^{\rm el}$, all the diagonal elements of $h_{n,n}$ become equal. Recalling that the matrix form of $H_{\rm eff}^{\rm el}$ is real symmetric tridiagonal, if $\{a_n^k\}$ $(n=1,\ldots,N)$ is an eigenvector of the matrix, then $\{(-1)^n a_n^k\}$ $(n=1,\ldots,N)$ should be another eigenvector of the matrix. This immediately implies that $a_n^+ = (-1)^n a_n^- \equiv a_n^0$, $D_n^+ = D_n^- = \frac{1}{2}$, and $\frac{1}{2}(P_n^+ + P_n^-) = P_n^v$, and self-consistency is obtained. The constant charge density is a result of Eq. (2), where the soliton (antisoliton) has equal probability to be positively (negatively) charged or negatively (positively) charged. The above analysis allows us to simplify our computation procedure. The equal constant elements of $h_{n,n}$ have no effect on the calculation except to shift the energy scale, so we set all the $h_{n,n}=0$ below.

The equation of motion is integrated within the adiabatic (Born-Oppenheimer) approximation. This approximation is justified by Monte Carlo simulation and the quantum fluctuation studies in the polyacetylene case if the Coulomb interaction strength U is less than $2t_0$.[24,25] This is reasonable since the ion mass is much greater than the electron mass and the Peierls gap is less than the optical-phonon energy.[26]

For convenience we define η_n, the staggered displacement order parameter, which is related to the real displacement u_n by

$$\eta_n = (-1)^{n-1} u_n \ . \tag{8}$$

The equation of motion reads

$$M\ddot{\eta}_n = K(2\eta_n + \eta_{n+1} + \eta_{n-1}) + F_n^{\rm el} \ , \tag{9a}$$

with

$$F_n^{\rm el} = -\frac{\partial}{\partial \eta_n} \langle \Psi_x \mid H^{\rm el} \mid \Psi_x \rangle \ . \tag{9b}$$

The major numerical problem is the calculation of the electron force term $F_n^{\rm el}$. We use the matrix form to illustrate our method. Suppose $\underline{H}$ is a real symmetric matrix, whose elements are functions of η_n and a_i^k, which are the elements of $\underline{A}$. If $\underline{A}$ is the transformation matrix, which is real orthogonal, and $\underline{\Lambda}$ is the diagonalized matrix, whose elements are λ_k, we have

$$\underline{\Lambda} = \underline{A}' \underline{H} \, \underline{A} \ , \tag{10a}$$

with

$$\underline{A}' \underline{A} = \underline{A} \, \underline{A}' = \underline{1} \ , \tag{10b}$$

where $\underline{A}'$ is the transpose matrix of $\underline{A}$. Differentiating both sides of Eq. (10a) with respect to η_n, we have

$$\frac{\partial \underline{\Lambda}}{\partial \eta_n} = \underline{A}' \frac{\partial \underline{H}}{\partial \eta_n} \underline{A} + \underline{G} \ , \tag{11a}$$

where the elements of $\underline{G}$ have the following form,

$$g_{k,p} = \sum_s \frac{\partial a_s^k}{\partial \eta_n} a_s^p (\lambda_p - \lambda_k) \ . \tag{11b}$$

Using the expression (6b) and the relation (10b) and noticing that the off-diagonal terms of $\partial \underline{\Lambda}/\partial \eta_n$ and the diagonal terms of G are all equal to zero, we derive the following expression for $\partial P_n^v / \partial \eta_n$,

$$\frac{\partial P_n^v}{\partial \eta_m} = \sum_l K_{n,l} \left[-\frac{\partial t_l}{\partial \eta_m} - V \frac{\partial P_l^v}{\partial \eta_m} \right] , \tag{12a}$$

with

$$K_{n,l} = \sum_{k,p} (a_n^k a_{n+1}^p + a_n^k a_{n+1}^p) \times \frac{1}{\lambda_k - \lambda_p} (a_l^k a_{l+1}^p + a_l^k a_{l+1}^p) \ , \tag{12b}$$

where the k sum is over all the occupied states and the p sum is over all the unoccupied states. From (12b) it is clear that $K_{n,l}$ are symmetric about n and l and only depend on the eigenvalues and the eigenvectors obtained from Eq. (7), so we only need to calculate them once for each time step prior to calculating the derivative. Then the derivatives of P_n^v with respect to different η_m can be obtained through a simple iteration method or by solving a system of linear equations. We should point out that the formulations of (12) are similar to the formulae from the first-order perturbation theory, except the expressions here for $\partial P_n^v / \partial \eta_m$ are exact. $\partial a_n^0 / \partial \eta_m$ can be calculated similarly. The use of Eq. (12) greatly reduces the CPU (central-processing unit) times and makes the present simulation possible.

As pointed by Kivelson and Heim,[6] the Hamiltonian in Eq. (1) is unstable with respect to a shrinking of the chain length in the presence of soliton pairs. We add an extra term in addition to the usual linear term[16] to avoid length shrinking:

$$H' = A \left[\sum_n (u_n - u_{n+1}) + S(u_1 - u_0)^2 + S(u_N + u_0)^2 \right] , \tag{13}$$

where the parameter A is determined by minimization of the energy with respect to the lattice constant in the perfectly dimerized ground state, and the parameter S is chosen to be 0.1 here. The effect of this extra S term is equivalent to that of adjointing a spring to each end of the chain. These terms do not affect the lattice distortion patterns in the calculation.

NUMERICAL RESULTS

We first study the potential energy in the presence of a soliton pair. In the continuum model[27] there is a solution

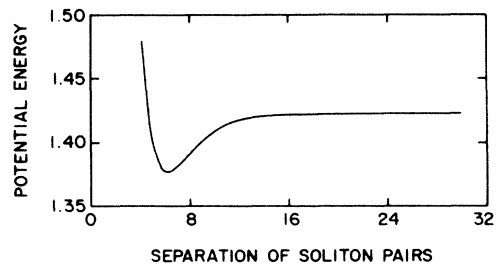

FIG. 1. Potential energy (in units of Δ_0) versus the separation of the soliton-antisoliton pairs, $2x_0$ (in units of the lattice constant a). The small potential well makes the vibration of an exciton possible.

for the lattice displacement patterns corresponding to a soliton-antisoliton pair which can be used approximately here,[28]

$$u(x)=u_0(1+k_0\xi_0\{\tanh[k_0(x-x_0)] -\tanh[k_0(x+x_0)]\}) , \quad (14a)$$

with

$$\xi_0=\frac{2t_0a}{\Delta_0};\ \tanh(2k_0x_0)=k_0\xi_0 , \quad (14b)$$

where ξ_0 is the coherence length, a is the lattice constant, Δ_0 is the gap parameter for the perfectly dimerized chain, u_0 is the magnitude of the uniform dimerization, $2x_0$ is the soliton-antisoliton separation, and k_0 is related to x_0 through Eq. (14b).

In Fig. 1, we plot the potential energy versus the separation of the soliton-antisoliton pair, $2x_0$. The curve can be described approximately by a function

$$V(x_0)=-\frac{c}{x_0}+\frac{d}{x_0^2} .$$

With analogy to classical mechanics, lattice relaxation after photoexcitation depends on the total energy gain. If the total energy is below the height of the potential well the excitation will be locally trapped. We perform our simulation for different total system energies.

The basic excitation for each simulation was the moving of an electron from the top of the valence band to the bottom of the conduction band, with an energy difference of $2\Delta_0$. (Owing to the Coulomb interaction, the total energy gain is smaller than $2\Delta_0$. For example, $E_t=1.963\Delta_0$, when $U=4.0$ eV and $V=1.5$ eV.) Two methods can be used to consider lowering total system energies. We can set all the velocities to zero after several time steps, or, instead of starting from a perfectly dimerized case, we can start from some other lattice configuration by means of Eq. (14). The first method may be interpreted as resulting from the emission of phonons during the relaxation process, and the latter can be related to the instanton approach,[29] wherein the lattice fluctuates owing to quantum effects before it absorbs a photon whose energy is less than $2\Delta_0$. The two methods are equivalent in the numerical calculation.

The simulations have been performed for different sets of U and V in a chain of 40 atoms. We focus on a typical set, $U=4.0$ eV and $V=1.5$ eV. The other parameters used here are $t_0=2.5$ eV, $\alpha=4.82$ eV/Å, $u_0=0.1$ Å, and $K=18.17$ eV/Å^2. The calculated gap parameter $\Delta_0=2.52$ eV, which is enlarged by the V term. The creation energy of the well-separated soliton-antisoliton pair is about $1.42\Delta_0$, and the creation energy of the excitonic bound state is about $1.37\Delta_0$. For these parameters

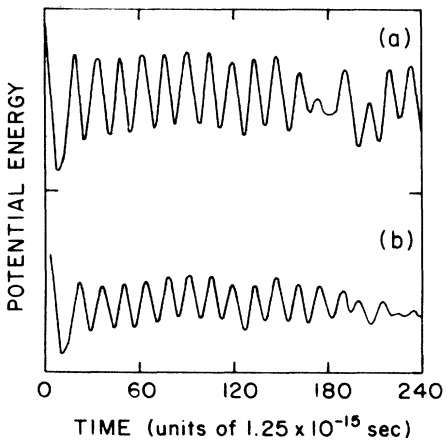

FIG. 2. Time evolution of the potential energy. The total energy of the curve (a): $E_t=1.963\Delta_0$ (initialized from the dimerized state); the curve (b): $E_t=1.7693\Delta_0$. For each curve the ranges of the ordinate is from $1.3\Delta_0$ to $2.0\Delta_0$.

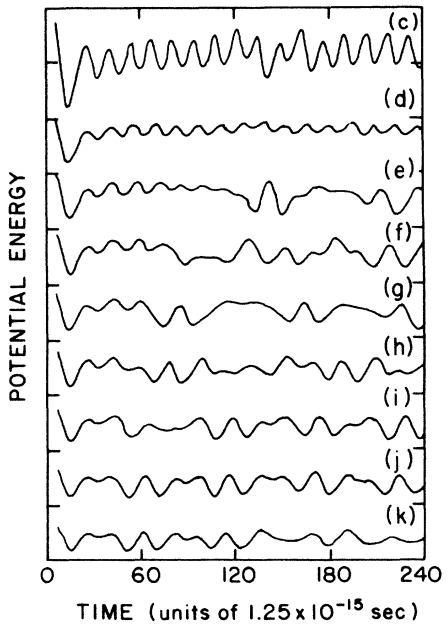

FIG. 3. As in Fig. 2. The curve (c): $E_t=1.5311\Delta_0$; (d): $E_t=1.4526\Delta_0$; (e): $E_t=1.4458\Delta_0$; (f): $E_t=1.4389\Delta_0$; (g): $E_t=1.4325\Delta_0$; (h): $E_t=1.4265\Delta_0$; (i): $E_t=1.4210\Delta_0$; (j): $E_t=1.4157\Delta_0$; and (k): $E_t=1.4110\Delta_0$. The range of the ordinate in each curve is from $1.35\Delta_0$ to $1.45\Delta_0$, except for the top one, which ranges from $1.35\Delta_0$ to $1.55\Delta_0$.

the dynamical simulations were performed under the following sets of system energies: (a) $E_t=1.963\Delta_0$ (initialized from the dimerized state), (b) $E_t=1.7693\Delta_0$, (c) $E_t=1.5311\Delta_0$, (d) $E_t=1.4526\Delta_0$, (e) $E_t=1.4458\Delta_0$, (f) $E_t=1.4389\Delta_0$, (g) $E_t=1.4325\Delta_0$, (h) $E_t=1.4265\Delta_0$, (i) $E_t=1.4210\Delta_0$, (j) $E_t=1.4157\Delta_0$, and (k) $E_t=1.4110\Delta_0$.

Because the dynamics are very sensitive to the system energy, we must ensure that the energy is conserved precisely during the calculation. We use a multistep method[30] to integrate the equation of motion so the calculated system energy fluctuates within $10^{-4}\Delta_0$ (i.e. the relative error of the energy is less than 10^{-6}). The time evolution of the system potential energy has different features for the different cases. We plot their behaviors in Figs. 2 and 3. Figure 2 has two curves representing case (a) and case (b). The ordinate of the figure represents the potential energy and ranges from $1.3\Delta_0$ to $2.0\Delta_0$ for each interval. Figure 3 has nine curves corresponding to cases (c)—(k) from the top to the bottom, respectively. The system energy is stepped down from the top to the bottom. Each interval of the ordinate is scaled from $1.35\Delta_0$ to $1.45\Delta_0$ except the top large one, which is scaled from $1.35\Delta_0$ to $1.55\Delta_0$.

We first consider the lower-energy curves, (i), (j), and (k). The system energies of these three cases are near or lower than the soliton pair energy. They clearly exhibit a periodic breather behavior. To see this in detail, we display the time evolution of the optical components of the staggered displacement order parameters,[19] which are defined as $y_n=\frac{1}{4}(2\eta_n+\eta_{n+1}+\eta_{n-1})$, in a typical cycle for case (j) in Figs. 4 and 5. In Fig. 4, we see that the exciton breather expands from the time $T=116$, via $T=125$ and $T=137$ to $T=144$ (in units of 1.25×10^{-15} sec), while the system potential energy goes from a local maximum through a local minimum and another local maximum, then to a shallow local minimum. In Fig. 5, we see that the breather shrinks from $T=144$ to 170, while the system potential energy goes through a similar sequence. The periodicity for case (k) is about 53, is about 54 for case (j), and is about 55 for case (i), corresponding to $\hbar\omega\approx500$ cm^{-1}, in agreement with the observed 500 cm^{-1} mode in the infrared.[13] (When $U=4.0$ eV and $V=3.0$ eV, the average periodicity is about 49.) It is also interesting to note from the Figs. 4 and 5 that there exists a small central breather feature around the local minimum energy configuration ($T=144$).

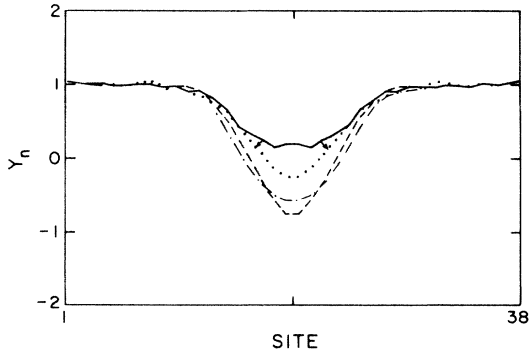

FIG. 4. Typical exciton-breather expansion cycle, for case (j) in Fig. 3 ($E_t=1.4157\Delta_0$). The abscissa is the site index n, and the ordinate is the optical components of the staggered displacement order parameters, y_n. The solid line, $T=116$ (in units of 1.25×10^{-15}); the dotted line, $T=125$; the dashed line, $T=137$; and the dot-dash line, $T=144$. The dotted line represents a lattice configuration which has a local minimum of the potential energy.

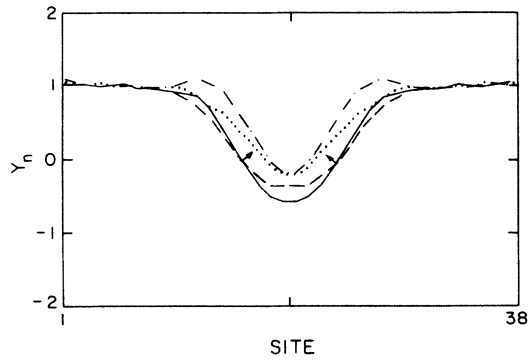

FIG. 5. (Follows Fig. 4). The exciton breather in contraction. The solid line, $T=144$; the dashed line, $T=150$; the dotted line, $T=161$ (a local minimum potential-energy configuration); and the dot-dash line, $T=170$.

Next we turn to cases (c) and (d). We see from Fig. 2 that the time evolution of the potential energy of these two curves has different features from that of curves (i), (j), and (k). We find no exciton-breather feature in this energy region, but rather a separated soliton-antisoliton pair is formed, and the central breather between the soliton-antisoliton pair appears. Diagrams of the process at different times for each case are plotted in Figs. 6 and 7. Figure 6 corresponds to case (d). The three curves represent the lattice configurations at $T=209$. $T=216$, and $T=223$, respectively, with the potential energy reaching a local minimum at $T=216$. We find the soliton-antisoliton is quite static, in a period of nearly 200 time steps the pair remains in the same positions, and only the

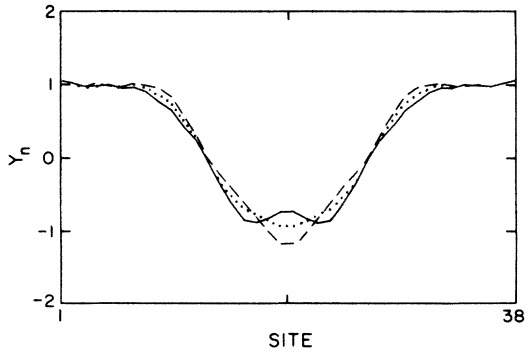

FIG. 6. A central-type breather is located between a quite static soliton-antisoliton pair. This is case (d) in Fig. 3 ($E_t=1.4526\Delta_0$). The solid line, $T=209$; the dotted line, $T=216$ (a local minimum potential-energy configuration); and the dashed line, $T=223$.

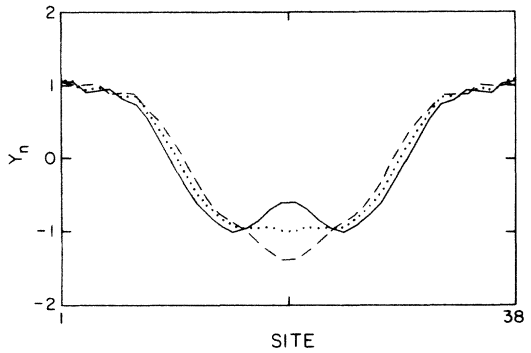

FIG. 7. A central-type breather is located between a well-separated soliton-antisoliton pair, which vibrates along the chain with a long periodicity. [$E_t = 1.5311\Delta_0$, corresponding to case (c) in Fig. 3.] The solid line, $T = 203$; the dotted line, $T = 210$ (a local minimum potential-energy distribution); and the dashed line, $T = 217$.

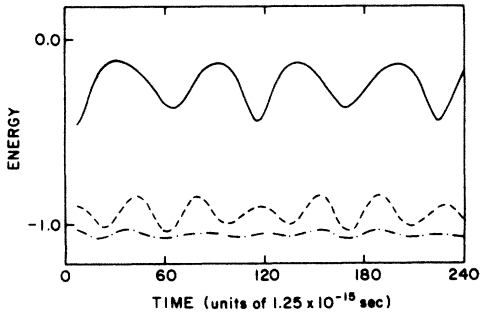

FIG. 8. Time dependence of the single electron-energy spectrum for case (j) ($E_t = 1.4157\Delta_0$). Only the top three levels below the gap center are plotted. The top level oscillates with the same frequency as that of the exciton breather. The second top level oscillates with a higher frequency than that of the top one.

central breather between them oscillates. Figure 7 corresponds to case (c), which has a higher system energy than that of case (d). We can see from the figure that the soliton-antisoliton pair now has large separation, but is still confined and has a large-scale vibration along the chain with a much longer periodicity than that of the central breather. The reason for the confinement is partially owing to the Coulomb attraction and is partially owing to the fact that the central breather consumes the excess energy, which would other wise appear as kinetic energy of the solitons.

The salient difference between the low-energy (Figs. 4 and 5) and high-energy (Figs. 6 and 7) cases is that the former depicts an exciton oscillating about the center of the chain while the latter depicts a fully formed soliton pair with an oscillating breather state superimposed upon them. It is clear that in the low-energy cases the oscillation is in the width of the distortion while in the high-energy cases the separation of the solitons may either remain fairly constant (Fig. 5) or may increase (Fig. 6), but the oscillating feature is that of the central atoms of the chain only.

In Figs. 8 and 9, we compare the time evolutions of the single electron spectra of cases (j) and (d). We plot only the top three levels below the gap center. In Fig. 9, the top state of case (d) becomes a midgap state owing to the appearance of the soliton-antisoliton pairs. The next state in the valence band is shifted into the gap and oscillates with the same frequency as the central breather. In Fig. 8, the top state for case (j) oscillates near the gap center with the same frequency as the exciton breather. We can conclude from the above descriptions that the two types of breathers have different origins. It is also interesting to note that the next state in the valence band for case (j) oscillates near the gap edge, but has a higher frequency than that of the exciton breather.

We consider higher system energies in cases (a) and (b). In these two cases (see Fig. 2), the soliton-antisoliton pairs are no longer confined, but are free to separate, leaving behind a central-breather oscillation. In comparing these two cases we find that the breather amplitude and the soliton velocity in case (a) are larger than those in case (b). In Fig. 2, we can see that the energy oscillations become weak at times near $T = 160$ in curve (a) and at times near $T = 220$ in case (b) because of the collisions of the soliton pairs. This also implies that the soliton velocity is higher in case (a) than in case (b).

Cases (e)—(h) are in a transition region with a mixture of the properties of cases (d) and (j). The vibration of the exciton breather slows and a central breather begins to appear as the system energy becomes large. We do not describe these cases here in detail.

We may summarize this section as follows: There are three major regions of different dynamical behavior depending on the total system energy. An exciton breather appears if the system energy is between the soliton pair-creation energy and the low-energy exciton state. As the system energy increases it is energetically favorable for the exciton breather to dissociate into a soliton-antisoliton pair. In this energy region the soliton-antisoliton pair forms, but is confined and oscillates along the chain with a large periodicity, and a central breather mode appears between the pair. At higher system energies, the soliton-antisoliton pair starts to separate, and the central breather still exists. This latter feature is also found in pure SSH

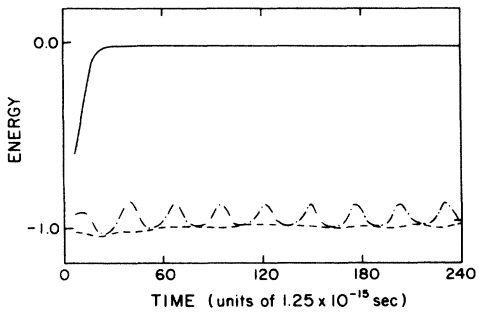

FIG. 9. (As in Fig. 8) time dependence of the single electron-energy spectrum for case (c) ($E_t = 1.5311\Delta_0$). The top level becomes a midgap state owing to the soliton-antisoliton pair, and the second top one oscillates near the gap edge with the central breather frequency.

model simulation,[19] so the main effect of including the Coulomb interaction is to introduce the possibility of photogeneration of an exciton-breather state.

DISCUSSION

It is worthwhile to point out that a similar result of finding it energetically possible to split the breather into a soliton-antisoliton pair has also been obtained in the driven sine-Gordon system by Lomdahl *et al.*[31] In their paper they concluded that large driving forces cause the breather to split into a kink-antikink pair while for small driving forces the breather enters stationary modes. This similarity gives us reason to believe that the exciton-breather state is an essential excitation in the SSH extended Hubbard model, and one would be able to obtain the explicit expression of the thresholds for the three regions described above if an analytical solution for the exciton breather is available.

The agreement of the exciton-breather vibration frequency with the observed infrared activity "pinning" mode at 500 cm^{-1} is a main result of this paper. However, the weak dependence of the exciton-breather frequency on the system energy suggests that the interpretation will survive the quantization of the exciton-breather energy. The dissociation temperature of the exciton into the oppositely charged soliton-antisoliton pairs was estimated to be 120 K by the calculation of the exciton binding energy.[8] We are unable to estimate this temperature from our dynamical simulations but we believe that the dissociation temperature can be obtained through quantization of the breather energy. The temperature dependency of the 500 cm^{-1} "pinning" mode and the photoconductivity are further evidence of the existence of the exciton breather. The overall neutral exciton breather is not able to give photoconductivity, but is the cause of the "pinning" mode. This is the reason that the 500 cm^{-1} mode and photoconductivity cannot "coexist" at the same temperature (see Fig. 2 of Ref. 13).

The strong temperature-dependent absorption peak (high-energy peak) at ~ 1.35 eV in the photoexcitation[32,33] has been a puzzle for a long time. Because the exciton breather will dissociate at high temperature, and also because both the second top level in the valence band and the second bottom level in the conduction band shift into the gap and oscillate (see Fig. 8), a natural interpretation should be to attribute this peak to the electronic transition between these two states. This peak has been interpreted as the electronic transition between the corresponding states in the presence of the central breather[19] (see Fig. 9). A possible solution is some sort of combination of the two interpretations. Noticing that the average energy difference between two gap edge states in the exciton-breather case is about $1.82\Delta_0$ which is smaller than that in the central breather case (about $1.88\Delta_0$), that the decay time of the exciton breather is expected to be short, and that the exciton breather is strongly temperature dependent, and in comparison with the experiment results,[32,33] we believe that the exciton breather plays a major role for the high-energy peak at low temperature and at short times while the central breather is responsible for the bleaching peak at high temperature and at long times.

ACKNOWLEDGMENT

One of us (C.L.W.) would like to thank Professor Melvin Lax for much stimulating advice and critical reading of this manuscript, and to thank Dr. Zhao Bin Su, Dr. Shirish Chitanvis, Dr. Wei Cai, and Dr. Boris Yudanin for their encouragement and helpful discussions. This work was supported in part by a grant from the U.S. Department of Energy (Office of Basic Energy Sciences, the Division of Material Sciences).

[1]H. Thomman, L. R. Dalton, Y. Tomkiewicz, N. S. Shiren, and T. C. Clarke, Phys. Rev. Lett. **50**, 533 (1983).
[2]S. Kuroda and H. Shirakawa, Solid State Commun. **43**, 591 (1982).
[3]A. J. Heeger and J. R. Schrieffer, Solid State Commun. **48**, 207 (1983).
[4]H. Thomman, L. R. Dalton, M. Grabowski, and T. C. Clarke, Phys. Rev. B **31**, 3141 (1985).
[5]K. R. Subbaswamy and M. Grabowski, Phys. Rev. B **24**, 2168 (1981).
[6]S. Kivelson and D. E. Helm, Phys. Rev. B **26**, 4278 (1982).
[7]J. E. Hirsch and M. Grabowski, Phys. Rev. Lett. **52**, 1713 (1984).
[8]M. Grabowski, D. Hone, and J. R. Schrieffer, Phys. Rev. B **31**, 7850 (1985).
[9]W. P. Su, J. R. Schrieffer, and A. J. Heeger, Phys. Rev. Lett. 1698 (1979); Phys. Rev. B **22**, 2099 (1980), **28**, 1138(E) (1983).
[10]M. J. Rice, Phys. Rev. Lett. **51**, 142 (1983).
[11]M. J. Rice and I. A. Howard, Phys. Rev. B **28**, 6089 (1983).
[12]B. R. Weinberger, Phys. Rev. Lett. **50**, 1693 (1983).
[13]G. B. Blanchet, C. R. Fincher, and A. J. Heeger, Phys. Rev. Lett. **51**, 2132 (1983).
[14]G. B. Blanchet, C. R. Fincher, T. C. Chung, and A. J. Heeger, Phys. Rev. Lett. **50**, 1938 (1983).
[15]J. Orenstein, Z. Vardeny, G. L. Baker, G. Eagle, and S. Etemad, Phys. Rev. B **30**, 786 (1984).
[16]W. P. Su and J. R. Schrieffer, Proc. Natl. Acad. Sci. USA **77**, 5626 (1980).
[17]E. J. Mele, Phys. Rev. B **26**, 6901 (1982).
[18]F. Guinea, Phys. Rev. B **30**, 1884 (1984).
[19]A. R. Bishop, D. K. Campbell, P. S. Lomdahl, B. Horovitz, and S. R. Phillpot, Phys. Rev. Lett. **52**, 671 (1984).
[20]C. L. Wang, Z. B. Su, and F. Martino, Phys. Rev. B **33**, 1512 (1986).
[21]J. D. Flood, E. Ehrenfreund, A. J. Heeger, and A. G. MacDiarmid, Solid State Commun. **44**, 1055 (1982).
[22]R. Ball, W. P. Su, and J. R. Schrieffer, J. Phys. (Paris) Colloq. **44**, C3-429 (1983).
[23]Z. B. Su and Lu Yu, Phys. Rev. B **27**, 5199 (1983).
[24]L. Falicov and F. Yudurain, J. Phys. C. **8**, 147 (1975).
[25]M. Nakahara and K. Maki, Phys. Rev. B **25**, 7789 (1982).
[26]S. A. Brazovskii and I. E. Dzyaloshinskii, Zh. Eksp. Teor. Fiz. **71**, 2338 (1976) [Sov. Phys.—JETP **44**, 1233 (1976)].
[27]H. Takayama, Y. R. Lin-liu, and K. Maki, Phys. Rev. B **21**,

2388 (1980).
[28]D. K. Campbell and A. R. Bishop, Nucl. Phys. **200**, 297 (1982); Phys. Rev. B **24**, 4859 (1981).
[29]J. P. Sethna and S. Kivelson, Phys. Rev. B **26**, 3513 (1982).
[30]W. E. Milne, Am. Math. Month **40**, 322 (1933).
[31]P. S. Lomdahl, O. H. Olsen, and M. R. Samuelsen, Phys. Rev. A **29**, 350 (1984).
[32]J. Orenstein and G. L. Baker, Phys. Rev. Lett. **49**, 1043 (1982).
[33]C. V. Shank, R. Yen, R. L. Fork, J. Orenstein, and G. L. Baker, Phys. Rev. Lett. **49**, 1660 (1982).